

Chapman University Chapman University Digital Commons

Biology, Chemistry, and Environmental Sciences
Faculty Articles and Research

Science and Technology Faculty Articles and
Research

5-8-2018

Predicting Spatial Patterns in Precipitation Isotope ($\delta^2\text{H}$ and $\delta^{18}\text{O}$) Seasonality Using Sinusoidal Isoscapes

Scott T. Allen
ETH Zurich

James W. Kirchner
ETH Zurich

Gregory R. Goldsmith
Chapman University, goldsmit@chapman.edu

Follow this and additional works at: https://digitalcommons.chapman.edu/sees_articles

 Part of the [Atmospheric Sciences Commons](#), [Biogeochemistry Commons](#), [Environmental Chemistry Commons](#), [Environmental Monitoring Commons](#), [Fresh Water Studies Commons](#), [Geochemistry Commons](#), [Hydrology Commons](#), [Other Chemistry Commons](#), [Other Earth Sciences Commons](#), [Other Oceanography and Atmospheric Sciences and Meteorology Commons](#), and the [Water Resource Management Commons](#)

Recommended Citation

Allen, S. T., Kirchner, J. W. & Goldsmith, G. R. (2018). Predicting spatial patterns in precipitation isotope ($\delta^2\text{H}$ and $\delta^{18}\text{O}$) seasonality using sinusoidal isoscapes. *Geophysical Research Letters*, 45. <https://doi.org/10.1029/2018GL077458>

This Article is brought to you for free and open access by the Science and Technology Faculty Articles and Research at Chapman University Digital Commons. It has been accepted for inclusion in Biology, Chemistry, and Environmental Sciences Faculty Articles and Research by an authorized administrator of Chapman University Digital Commons. For more information, please contact laughtin@chapman.edu.

Predicting Spatial Patterns in Precipitation Isotope ($\delta^2\text{H}$ and $\delta^{18}\text{O}$) Seasonality Using Sinusoidal Isoscapes

Comments

This article was originally published in *Geophysical Research Letters*, volume 45, in 2018. DOI: [10.1029/2018GL077458](https://doi.org/10.1029/2018GL077458)

Copyright

American Geophysical Union



Geophysical Research Letters

RESEARCH LETTER

10.1029/2018GL077458

Key Points:

- Sine curves can capture seasonal cycles in precipitation $\delta^{18}\text{O}$, $\delta^2\text{H}$, and, to a lesser extent, line-conditioned excess
- The parameters describing these seasonal sine curves can be interpolated spatially, allowing isotope predictions in space and time
- Prediction errors and biases differ among precipitation isotope mapping methods that use different calibration time steps

Supporting Information:

- Supporting Information S1

Correspondence to:

S. T. Allen,
allensc@ethz.ch

Citation:




Allen, S. T., Kirchner, J. W., & Goldsmith, G. R. (2018). Predicting spatial patterns in precipitation isotope ($\delta^2\text{H}$ and $\delta^{18}\text{O}$) seasonality using sinusoidal isoscapes. *Geophysical Research Letters*, 45. <https://doi.org/10.1029/2018GL077458>

Received 5 FEB 2018

Accepted 2 MAY 2018

Accepted article online 8 MAY 2018

Predicting Spatial Patterns in Precipitation Isotope ($\delta^2\text{H}$ and $\delta^{18}\text{O}$) Seasonality Using Sinusoidal Isoscapes

Scott T. Allen^{1,2} , James W. Kirchner^{1,3} , and Gregory R. Goldsmith^{2,4} 

¹Department of Environmental Systems Science, ETH Zurich, Zurich, Switzerland, ²Ecosystem Fluxes Group, Laboratory for Atmospheric Chemistry, Paul Scherrer Institute, Villigen, Switzerland, ³Swiss Federal Research Institute WSL, Birmensdorf, Switzerland, ⁴Schmid College of Science and Technology, Chapman University, Orange, CA, USA

Abstract Understanding how precipitation isotopes vary spatially and temporally is important for tracer applications. We tested how well month-to-month variations in precipitation $\delta^{18}\text{O}$ and $\delta^2\text{H}$ were captured by sinusoidal cycles, and how well spatial variations in these seasonal cycles could be predicted, across Switzerland. Sine functions representing seasonal cycles in precipitation isotopes explained between 47% and 94% of the variance in monthly $\delta^{18}\text{O}$ and $\delta^2\text{H}$ values at each monitoring site. A significant sinusoidal cycle was also observed in line-conditioned excess. We interpolated the amplitudes, phases, and offsets of these sine functions across the landscape, using multiple linear regression models based on site characteristics. These interpolated maps, here referred to as a sinusoidal isoscape, reproduced monthly observations with prediction errors that were smaller than or similar to those of other isoscapes. Sinusoidal isoscapes are likely broadly useful because they concisely describe seasonal isotopic behavior and can be estimated efficiently from sparse or irregular data.

Plain Language Summary Naturally occurring isotopic variations in precipitation are used to trace water movement through landscapes and ecosystems. However, direct measurements are often unavailable, so many isotope-based approaches to studying terrestrial processes require predicted isotopic inputs. We found that the isotopic composition of precipitation follows a predictable seasonal pattern. We developed a new approach for mapping precipitation isotope seasonality that will be useful in a wide range of fields.

1. Introduction

Accurately estimating the isotopic composition of precipitation (δ_p) is essential for many ecological and hydrological applications, including (for example) determining streamflow sources (Cable et al., 2011), estimating evapotranspiration rates (Jasechko et al., 2013), reconstructing climate from the isotopic variations in tree rings (McCarroll & Loader, 2004), or tracking animal migration (Hobson & Wassenaar, 2008). However, precipitation isotope measurements are difficult and costly; thus, direct measurements of δ_p are rarely available when and where they are needed. This is particularly the case for applications that require reconstructing the isotopic composition of past precipitation inputs. Where direct measurements are unavailable, there is a need for methods that can accurately predict or interpolate δ_p in their place (e.g., Sánchez-Murillo & Birkel, 2016).

Precipitation isotopes are often estimated through correlations with climate and geography, because the complexity of the underlying processes makes mechanistic predictions problematic. However, simple correlates such as temperature and precipitation amount (Rozanski et al., 1993) are often poor predictors of δ_p because they fail to account for the effects of changing moisture sources and air mass trajectories (Bowen, 2008; Kern et al., 2014; Liu et al., 2010). So-called continental, latitude, and amount effects (Ingraham, 1998) may be largely driven by how precipitation forms (e.g., Aggarwal et al., 2016). Geographic variations in the factors driving precipitation isotopic variations are partly reflected in maps of δ_p , commonly termed precipitation isoscapes (Bowen et al., 2009). Precipitation isoscapes are often constructed from long-term mean annual or monthly observations, interpolated using correlates or geostatistical relationships to yield a spatially continuous map of δ_p . However, these spatial patterns are not temporally constant, so spatial variations in δ_p at any specific time are unlikely to match (in either absolute or relative values) the mean annual pattern, or even the respective mean monthly spatial pattern. Thus, estimating δ_p from temporally integrated spatial patterns can yield errors in subsequent applications, such as tracing (or “assigning”) samples back to their point of origin (Vander Zanden et al., 2014). In applications where finer-scale variations are important, isoscapes can be constructed at higher temporal resolution.

Seasonal cycles in δ_p can follow a sinusoidal pattern, especially in midlatitude regions (Dutton et al., 2005; Vachon et al., 2007; Wilkinson & Ivany, 2002), so the spatial interpolation of parameters describing sine functions could hypothetically provide an efficient and accurate method for simultaneously mapping δ_p variations in both space and time (Jasechko et al., 2016). Such a “sinusoidal isoscape” is likely to be feasible, because the sine parameters that describe seasonal cycles in δ_p (i.e., the amplitude, phase, and mean value) have been shown to vary systematically across landscapes (Dutton et al., 2005; Halder et al., 2015; Vachon et al., 2007). Where seasonal patterns in δ_p are predominantly sinusoidal, and consistent from year to year, sinusoidal isoscapes provide a simple alternative to the monthly regression-modeling approach tested by Delavau et al. (2015).

Beyond simply predicting δ_p at specific times, the sine parameters (amplitude, phase, and offset) that are mapped by sinusoidal isoscapes may be useful for characterizing seasonal isotopic cycles and their propagation through hydrological and ecological systems. The offset defines the center of a modeled sinusoidal signal, which more accurately reflects the central tendency of the data than the mean or median when the sampling is uneven. The amplitude of the modeled sinusoid is a measure of the strength of the seasonal cycle in δ_p . As seasonal isotope cycles propagate through ecosystems or catchments, the dampening of amplitudes can indicate dispersion and mixing and therefore provide insight into the shape of transit time distributions (Kirchner, 2016a). The phase of the modeled sinusoid expresses when its peak values occur, and phase shifts between inputs and outputs can indicate advective transport rates. While these sinusoidal parameters have been used in diverse hydrological applications, they may also be useful in studying the transport of water isotopes through biological systems.

Sinusoidal functions may also be useful for capturing oscillations in the covariation of $\delta^2\text{H}$ and $\delta^{18}\text{O}$. The two isotope ratios are generally collinear, with a global mean relationship of roughly $\delta^2\text{H} = 8 \times \delta^{18}\text{O} + 10$, called the global meteoric water line. Deviations from this global relationship are often described as deuterium excess values (Dansgaard, 1964). The covariation of $\delta^2\text{H}$ and $\delta^{18}\text{O}$ at individual sites is expressed by local meteoric water lines (LMWLs) that better characterize site-specific precipitation than the global meteoric water line. Deviations of individual points from these LMWLs are termed line-conditioned excess or LC-excess (Landwehr & Coplen, 2006). Most precipitation will lie close to the LMWL and thus will have an LC-excess of nearly zero. As waters evaporate, they will become enriched in heavy isotopes such that they move off of the LMWL, and their LC-excess values will become negative. Thus LC-excess is a widely useful indicator of evaporation in ecosystems. However, precipitation itself can also deviate from the LMWL, and thus have nonzero LC-excess; these deviations (and deuterium excess variations) have been commonly attributed to variations in moisture sources, air mass trajectories, and cloud processes (e.g., Dansgaard, 1964), but the relative importance of these factors is debated (Martin et al., 2018; Pfahl & Sodemann, 2014). Variations in LC-excess within or between individual precipitation events are often unimportant because they will be damped as waters from these events are mixed together in the landscape. However, longer-lived (e.g., seasonal) variations in precipitation LC-excess may persist in soils and biota, and be misinterpreted as evaporation signals. Thus, quantifying seasonal variations in precipitation LC-excess establishes a baseline for inferring evaporative fractionation from LC-excess measurements in landscapes and ecosystems.

Here we compare sinusoidal isoscapes and several other approaches for predicting spatiotemporal variations in precipitation $\delta^{18}\text{O}$ and $\delta^2\text{H}$, using publicly available data from Switzerland and neighboring countries, a region noted for steep terrain and complex patterns of atmospheric transport (Frei et al., 2003; Kern et al., 2014). We first evaluate how well sine functions explain $\delta^{18}\text{O}$, $\delta^2\text{H}$, and LC-excess observations and how well their parameters are explained by spatial predictor variables. We then compare the predictive accuracy of sinusoidal isoscapes against several other approaches for estimating precipitation $\delta^{18}\text{O}$ and $\delta^2\text{H}$.

2. Methods

2.1. Data

Monthly precipitation isotope data were assembled in March 2017 from the Global Network of Isotopes in Precipitation (GNIP; International Atomic Energy Agency/World Meteorological Organization, 2018), the Austrian Network of Isotopes in Precipitation (ANIP; Water Information System Austria, 2018), and the Swiss National Groundwater Monitoring Isotope Module (NAQUA-ISOT; data are available at International

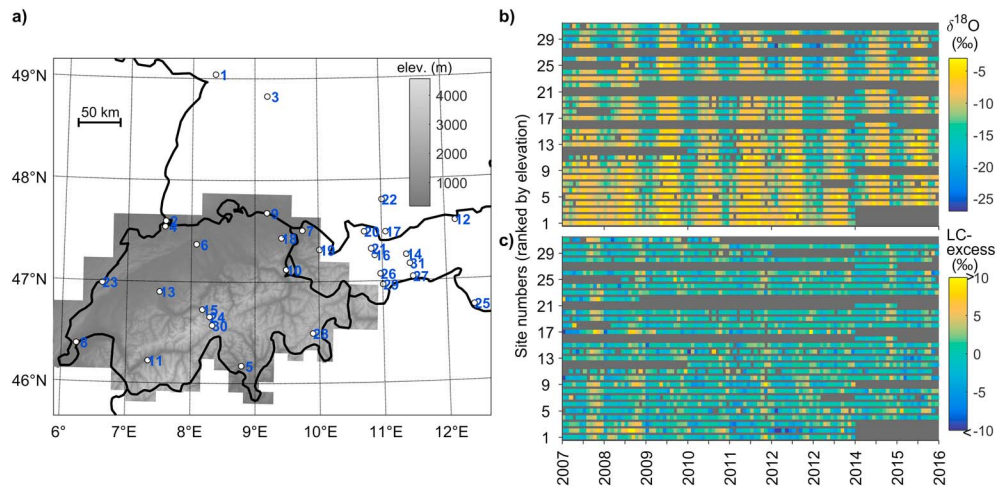


Figure 1. Temporal patterns in precipitation $\delta^{18}\text{O}$ and LC-excess across our study sites. (a) Map of precipitation isotope monitoring sites, with site numbers ranked by elevation. (b) Monthly variations in $\delta^{18}\text{O}$ exhibit seasonal cycles—low in winter and high in summer—that vary with elevation. (c) Monthly variations in LC-excess also exhibit seasonal cycles, but with different phases (high in fall and low in spring) than those of $\delta^{18}\text{O}$.

Atomic Energy Agency/World Meteorological Organization, 2018). The final data set included precipitation $\delta^{18}\text{O}$ and $\delta^2\text{H}$ measured at 13 sites in Switzerland and an additional 18 Austrian and German sites within 135 km of the Swiss border (Figure 1a). These sites span elevations ranging from 112 to 2,245 m above sea level, mean annual precipitation rates ranging from 60 to 207 cm/year, and mean annual temperatures ranging from 0.4 to 12.4 °C (Table S1). A period with high temporal coverage (January 2007 to December 2015) was selected; however, there were still gaps that varied by site (Figure 1b). Monthly precipitation amounts and mean temperatures were also acquired from collocated or nearby weather stations (Table S1). For spatial mapping, we also used 200-m resolution gridded layers of monthly means (1981–2010) of precipitation and temperature (MeteoSwiss, Zurich, Switzerland) and a 200-m resolution digital elevation map (Swisstopo, Bern, Switzerland); all gridded outputs were calculated at 200-m resolution. Geographic analyses were conducted in UTM coordinates (zone 32).

2.2. Analysis of Sinusoidal Variations in Precipitation Isotopic Composition

Sine curves (described by the parameters *amplitude*, phase [φ], and *offset*) were fitted to monthly, empirical $\delta^{18}\text{O}$ and $\delta^2\text{H}$ time series from each site. An additive model of sine and cosine functions with a fixed period of one year was fitted with two amplitude parameters, a_1 and a_2 , and a constant offset parameter, *offset*:

$$\text{Precipitation } \delta^{18}\text{O} \text{ or } \delta^2\text{H} (t) = a_1 \times \cos(2\pi t) + a_2 \times \sin(2\pi t) + \text{offset}. \quad (1)$$

These fitted parameters were used to define a sine curve,

$$\text{Precipitation } \delta^{18}\text{O} \text{ or } \delta^2\text{H} (t) = \text{amplitude} \times \sin(2\pi t - \varphi) + \text{offset}, \quad (2)$$

with phase φ calculated as

$$\varphi \text{ (radians)} = -\text{atan2}(a_1, a_2), \text{ or, as peak day of year} = 365 \frac{\text{days}}{\text{year}} \left(\frac{1}{4} + \frac{\varphi}{2\pi} \right), \quad (3)$$

and with amplitude calculated as

$$\text{amplitude} = \sqrt{a_1^2 + a_2^2}. \quad (4)$$

Time, t , is defined in decimal years. Sine parameters and fit statistics for $\delta^{18}\text{O}$, $\delta^2\text{H}$, and LC-excess (defined below) for all observation sites are in Table S2. Standard errors of amplitudes and φ were calculated from the uncertainties in a_1 and a_2 using Gaussian error propagation. Equivalent parameter values and uncertainties were also obtained by nonlinear fitting using the “nlinfit” algorithm in MATLAB R2016B (Mathworks, Natick, Massachusetts, USA).

Potential relationships between these sine parameters and spatial predictors (elevation, latitude, longitude, mean annual precipitation, and mean annual range of monthly temperatures) at δ_p measurement sites

were examined through multiple regression. While more mechanistic factors could have been incorporated (e.g., seasonal atmospheric circulation patterns), our goal was to use simple, widely available data. Among predictor variables, the strongest collinearity was between elevation and temperature range with a Pearson correlation coefficient of only -0.4 (Table S3). We used a stepwise model selection approach based on minimizing the Akaike information criterion to include or omit each predictor variable. This regression routine was applied using the “stepwiselm” function, implemented with and without robust fitting in MATLAB R2016B. Robust and nonrobust fitting yielded functionally equivalent results. To test how well the sine functions represented temporal variations, residuals from each curve were quantified and then compared across sites for both $\delta^{18}\text{O}$ and $\delta^2\text{H}$. Residuals from the fitted sine curves were also tested for spatial autocorrelation.

Spatiotemporal variations in site-specific relationships between $\delta^2\text{H}$ and $\delta^{18}\text{O}$ were also examined by observing the monthly deviations from the LMWL for each site. These deviations were described in terms of LC-excess, where $\text{LC-excess} = \delta^2\text{H} - b_1 \times \delta^{18}\text{O} - b_0$ (Landwehr & Coplen, 2006), where b_1 and b_0 are the slope and intercept of the LMWL, as estimated by the unweighted, orthogonal-least-squares fit to the relationship between $\delta^2\text{H}$ and $\delta^{18}\text{O}$ at each site. LC-excess differs from deuterium excess because deuterium excess variations can result from departures from the LMWL or from variations along a LMWL that has a slope different from 8. Therefore, LC-excess is better for interpreting deviations from LMWLs that differ among sites. Here the study-wide LMWL slope was 8.09 and the intercept was 9.43‰. We also calculated LMWLs for each individual site; their slopes varied among sites from 7.7 to 8.4, and their intercepts varied from 2 to 15‰. Seasonal cycles in LC-excess were quantified by fitting sine curves to LC-excess observations, following the same procedure used for $\delta^2\text{H}$ and $\delta^{18}\text{O}$ (equations (1)–(4)). We examined whether these hypothesized seasonal cycles varied spatially and whether those spatial variations could be explained by multiple linear regression with elevation, latitude, longitude, mean total annual precipitation, and mean annual range of monthly temperatures.

2.3. Comparison of Isoscape Methods for Predicting Precipitation Isotopic Composition

To assess the predictability of precipitation $\delta^{18}\text{O}$ by sine curves, we compared the prediction errors to those resulting from five other methods:

1. *Long-term mean* isoscape: a single, temporally integrated map of spatial variations in mass-weighted long-term mean precipitation $\delta^{18}\text{O}$. We calculated mass-weighted long-term mean $\delta^{18}\text{O}$ values for every measurement station by first determining the monthly mean $\delta^{18}\text{O}$ for each of the 12 months (over the 2007–2015 record), and then weighting each monthly mean $\delta^{18}\text{O}$ by the corresponding mean monthly precipitation amount. We then used stepwise linear regression to determine the site characteristics (latitude, longitude, elevation, mean annual total precipitation, and seasonal temperature range) to be fitted to the weighted long-term means for the 31 sites. The spatial regression parameters were then used to model a spatial map of weighted long-term mean $\delta^{18}\text{O}$. Finally, we kriged the residuals (observed-modeled weighted long-term means) to create a layer that was added to the initial regression-based map of $\delta^{18}\text{O}$.
2. *Mean monthly* isoscapes: a set of 12 maps of mean monthly precipitation $\delta^{18}\text{O}$, temporally integrated across years for each month. We calculated mean $\delta^{18}\text{O}$ values (over the 2007–2015 record) for each of the 12 months for every measurement station. Then, for each of the 12 months, we used stepwise linear regression to determine the site characteristics (latitude, longitude, elevation, mean annual precipitation, and seasonal temperature range) to be fitted to the monthly mean $\delta^{18}\text{O}$ values for the 31 sites. The spatial regression parameters were then used to model a spatial map of each monthly mean $\delta^{18}\text{O}$. Finally, we kriged the residuals (observed-modeled monthly means) to create a layer that was added to the initial regression-based map of $\delta^{18}\text{O}$ for each month.
3. *Sinusoidal* isoscape: a set of three maps of the sine function parameters (amplitude, ϕ , and offset) representing the seasonality of precipitation $\delta^{18}\text{O}$. We fitted sine curves to the $\delta^{18}\text{O}$ time series from each measurement station (as described in section 2.2 above). We then used stepwise linear regression to determine the site characteristics (latitude, longitude, elevation, mean annual precipitation, and seasonal temperature range) to be fitted to the amplitude, ϕ , and offset values at the 31 sites. The spatial regression parameters were then used to model spatial maps of the amplitude, ϕ , and offset of the seasonal $\delta^{18}\text{O}$ cycles (e.g., Figure 2).

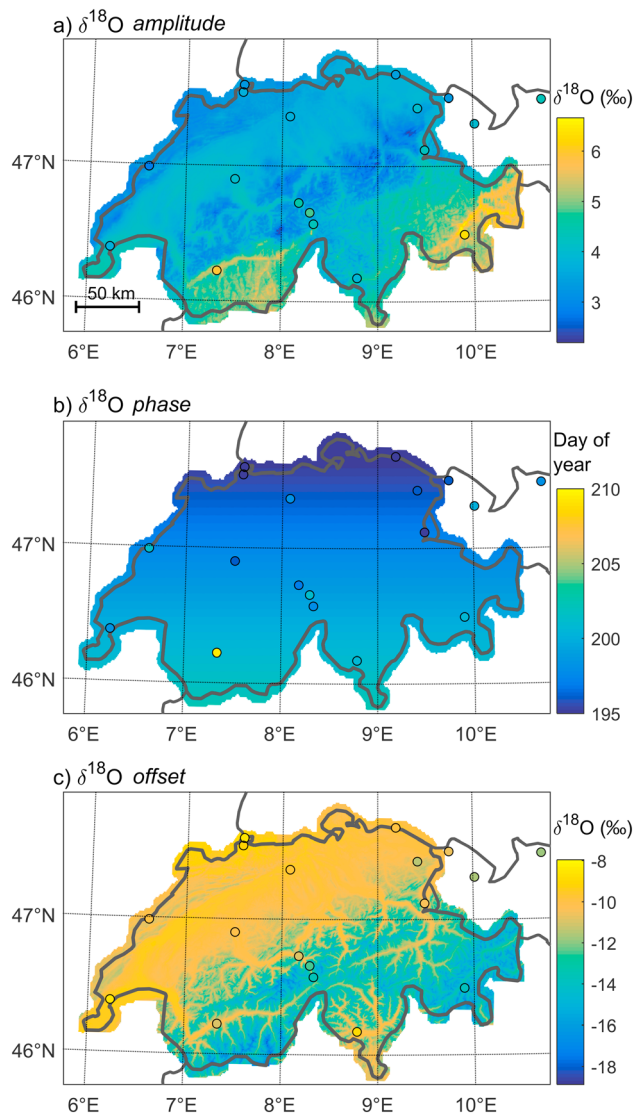


Figure 2. A sinusoidal isoscape of Switzerland, with maps of sine parameters that describe the seasonal dynamics in precipitation $\delta^{18}\text{O}$: (a) amplitude, (b) day of peak $\delta^{18}\text{O}$ associated with phase ϕ , and (c) offset of the cycle from $\delta^{18}\text{O} = 0$. The circles indicate the monitoring sites with colors showing parameter values for sine curves fitted to local observations. Values at elevations above 2,245 m, the elevation of the highest measurement station, or at annual precipitation amounts exceeding 207 cm, the highest value at a measurement station, should be interpreted with caution.

4. *Sinusoidal + monthly kriging* isoscape: monthly maps of precipitation $\delta^{18}\text{O}$ estimates (comprising 108 individual maps for 2007–2015). Building on the sinusoidal isoscape, we kriged the residuals (observed-modeled monthly $\delta^{18}\text{O}$) for each month to create monthly adjustment layers that are added to the sinusoidal isoscape.
5. *Individual-month* isoscape: monthly maps of precipitation $\delta^{18}\text{O}$ estimates (comprising 108 maps for 2007–2015). For each month, we used stepwise linear regression to determine the site characteristics (latitude, longitude, elevation, mean annual precipitation, and seasonal temperature range) to be fitted to monthly $\delta^{18}\text{O}$ measurements at the 31 sites. The spatial regression parameters were then used to model a spatial map of $\delta^{18}\text{O}$ for each month.
6. *Individual-month + monthly kriging*: monthly maps of precipitation $\delta^{18}\text{O}$ estimates (comprising 108 maps for 2007–2015).

Building on the individual-month isoscape, we kriged the residuals (observed-modeled $\delta^{18}\text{O}$) from each month's regression model to create a layer that was added to the corresponding monthly regression-based map of precipitation $\delta^{18}\text{O}$.

The kriging steps were tested using different numbers of bins and different variogram models; the results were relatively insensitive to these choices. For simplicity and reproducibility, all reported kriging steps were implemented using 10 bins (with a cutoff of one third of the maximum lag distance) and an exponential variogram model.

To assess the predictability of precipitation $\delta^{18}\text{O}$ derived from the six isoscape methods outlined above, a leave-one-out approach was used: isoscapes were iteratively generated using input data from all sites but one, and then used to predict $\delta^{18}\text{O}$ at the excluded site. The $\delta^{18}\text{O}$ prediction was then compared with the excluded $\delta^{18}\text{O}$ measurement. This procedure was repeated for each of the 31 sites and each of the six models. Each model was evaluated at each of its respective time steps: once for the long-term mean isoscape, 12 times for the mean monthly isoscapes, once for the sinusoidal isoscape, and 108 times for the three monthly isoscape methods. The mean absolute error, averaged across all 31 sites and then all 108 months, was used as a summary measure of the prediction error associated with each method (Figure 3). As a summary measure of prediction bias, we also calculated the *absolute mean error* (that is, the average, over all 108 months, of the absolute value of the mean error over all 31 sites; Figure 3). The spatial regression models and their relative performances were similar for $\delta^{18}\text{O}$ and $\delta^2\text{H}$ (Table S4), so here we present only $\delta^{18}\text{O}$.

We do not test the predictability of LC-excess using sinusoidal isoscapes or other methods. We did not pursue this step because site characteristics were poor predictors of the spatial variations in LC-excess seasonality.

3. Results

3.1. Analysis of Sinusoidal Variations in Precipitation $\delta^{18}\text{O}$, $\delta^2\text{H}$, and LC-Excess

At all sites, the seasonal precipitation cycles of heavier isotopes in summer and lighter isotopes in winter (Figures 1b and S2) were well approximated by sine functions. Site-specific statistics for these sine functions are given in Table S2. Fitted amplitudes varied from 2.6 to 6.4‰ in $\delta^{18}\text{O}$ and from 19.6 to 52.4‰ in $\delta^2\text{H}$ and were generally lower at lower elevations (Figure 1b). Peak values for fitted sine curves occurred between day of year 186 and 211 (late June through July). The offset parameter varied from -8.0 to -14.1 ‰ for $\delta^{18}\text{O}$ and

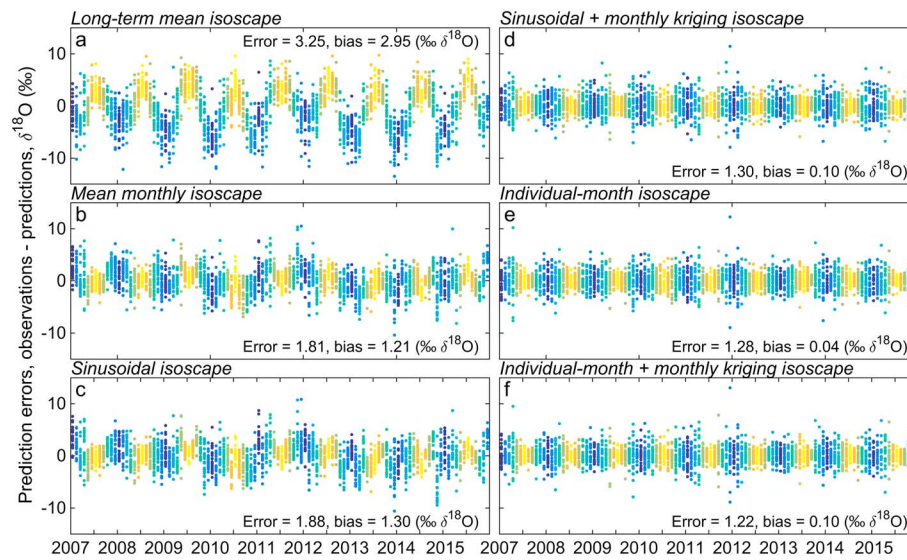


Figure 3. Distributions of prediction errors (observations-predictions) in predicted monthly $\delta^{18}\text{O}$ of precipitation for 31 measurement sites. $\delta^{18}\text{O}$ values were predicted for each site using only data from the other 30 sites (i.e., a leave-one-out approach to separate calibration and validation data sets). The color gradient illustrates time of year (lightest yellow for July and the darkest blue for January). The long-term mean isoscape cannot capture seasonal isotope cycles, and thus, its (a) prediction errors were distinctly larger than those from the (b) mean monthly and (c) sinusoidal isoscapes. Those isoscapes are not calibrated to each month individually, and thus, they cannot account for monthly anomalies that are captured by the (d) sinusoidal + monthly kriging, (e) individual-month, and (f) individual-month + monthly kriging isoscapes. Those that account for monthly anomalies have smaller errors (mean absolute deviation; section 2.3), and much lower biases (absolute mean deviation; section 2.3).

from -54.8 to -103.7‰ for $\delta^2\text{H}$, with lower values at higher elevations (Figure 1b). The R^2 values of the fitted sinusoidal cycles varied among sites from 0.47 to 0.94 (0.65 ± 0.10 ; mean \pm 1SD), with root-mean-square errors of $2.2 \pm 0.4\text{‰}$ $\delta^{18}\text{O}$ and $18.0 \pm 2.7\text{‰}$ $\delta^2\text{H}$. Mean absolute deviations from the sinusoidal cycles were 53% larger in winter than in summer. $\delta^{18}\text{O}$ and $\delta^2\text{H}$ deviations were often similar among nearby sites; in 59 of the 108 months analyzed, semivariogram models explained $>50\%$ of the variation in the residuals from the fitted sine curves, with a mean autocorrelation range of 93 km.

Multiple regression models of site characteristics explained much of the spatial variation in the sine parameters that describe the seasonal cycles of precipitation $\delta^{18}\text{O}$ and $\delta^2\text{H}$ (Table S4). Site characteristics explained most of the variability in amplitude (R^2 of 0.82 and 0.84 for $\delta^{18}\text{O}$ and $\delta^2\text{H}$) and offset (R^2 of 0.87 and 0.84 for $\delta^{18}\text{O}$ and $\delta^2\text{H}$). Although site characteristics only accounted for a small fraction of the variability in φ , the regression model root-mean-square error was small because φ values did not vary much (Table S4). Residuals from these linear models were not spatially autocorrelated (Moran's $I < 0.1$ and $p > 0.3$ for amplitude, φ , and offset). The regression parameters were used to generate the maps describing the sinusoidal isoscape of $\delta^{18}\text{O}$, as shown in Figure 2. The regression models and their associated statistics were similar for $\delta^2\text{H}$ and resulted in similar interpolated maps of the sinusoidal isoscape of $\delta^2\text{H}$ (Figure S2).

LC-excess in precipitation also varied seasonally (Figure 1c). Despite the strong collinearity between $\delta^{18}\text{O}$ and $\delta^2\text{H}$ values, the slight phase shifts in their seasonal cycles resulted in seasonal patterns in LC-excess. These LC-excess seasonal patterns could also be partially approximated by sine curves, with R^2 values varying from 0.05 to 0.51 (mean of 0.24 ± 0.11). The statistical significance of the sinusoidal cycle in LC-excess was $p < 0.001$ at 25 of the 31 monitoring sites. LC-excess amplitude varied from 0.7 to 3.6‰ (mean of $1.7 \pm 0.6\text{‰}$) with standard errors that averaged one-fourth of the amplitude itself. These amplitude values demonstrate a substantial seasonal oscillation in the relationship between $\delta^{18}\text{O}$ and $\delta^2\text{H}$ that is not captured by the LMWLs. Peak LC-excess mostly occurred in the autumn (day of year 257 to 316), lagging the peak in $\delta^{18}\text{O}$ by 92 ± 13 days (mean \pm standard deviation). Spatial variations in the sine parameters of the LC-excess seasonal cycles were not well explained by multiple regression models of site characteristics (Table S4); the R^2 values for these LC-excess regression models were 0.26 and 0.21 for amplitude and offset. There were no statistically significant predictors of φ ($p > 0.1$). Although these results demonstrate measurable seasonal cycles

in LC-excess, we did not map a sinusoidal isoscape for LC-excess because the parameters describing these seasonal cycles were not strongly explained by the site characteristics we examined.

3.2. Comparison of Isoscape Methods for Predicting Precipitation $\delta^{18}\text{O}$ and $\delta^2\text{H}$

The mean absolute error in predicting monthly values of precipitation $\delta^{18}\text{O}$ was, unsurprisingly, larger for isoscape methods that generated predictions at coarser time scales. The sinusoidal and mean monthly isoscapes, which incorporate seasonal dynamics, had 42 and 44% smaller errors, respectively, in predicting monthly precipitation $\delta^{18}\text{O}$ than the long-term mean isoscape did (Figure 3). The three approaches using monthly calibrations (sinusoidal + monthly kriging, individual-month, and individual-month + monthly kriging) further reduced the mean absolute error by 28–35%, compared to the approaches that only represented seasonal dynamics (sinusoidal and mean monthly isoscapes; Figure 3). Of these, the two methods that used a monthly kriging step, sinusoidal + monthly kriging and individual-month + kriging methods, did not have significantly smaller errors (1.30 and 1.22‰ $\delta^{18}\text{O}$, respectively) than the simpler individual-month isoscape (mean of 1.28‰ $\delta^{18}\text{O}$). The long-term and, to a lesser degree, the mean monthly and sinusoidal isoscapes frequently resulted in individual months with substantial prediction bias (Figures 3a–3c); those biases were almost entirely eliminated in the isoscapes using monthly calibration (Figures 3d–3f), as an inevitable consequence of separately fitting each monthly model to the data. However, those considering using the individual-month or individual-month + monthly kriging approaches should note that they are data-hungry and also potentially unstable, as demonstrated by the erratic regression coefficients that often changed sign from one month to the next (Figure S1). Furthermore, the stepwise model selection algorithm yielded regression models that included different variables in different months (Table S5 and Figure S1).

4. Discussion

Our results demonstrate that sine curves can represent seasonal cycles in precipitation $\delta^{18}\text{O}$, $\delta^2\text{H}$, and, to a lesser extent, LC-excess (Figure 1). Seasonal sine curves can be used to predict precipitation $\delta^{18}\text{O}$ and $\delta^2\text{H}$ because their parameters can be modeled as functions of site characteristics using multiple regression. These regression relationships facilitate mapping of seasonal variations in precipitation isotopes (i.e., the sinusoidal isoscape; Figure 2). By accounting for monthly deviations from these seasonal patterns, monthly $\delta^{18}\text{O}$ and $\delta^2\text{H}$ values of precipitation can be predicted more accurately than by sine-curve-based models alone (Figure 3).

The seasonal cycles of precipitation $\delta^{18}\text{O}$ and $\delta^2\text{H}$ observed here were correlated with site characteristics including latitude, longitude, elevation, total annual precipitation, and annual temperature range. However, these correlations are different in other regions. For example, across the GNIP data set, seasonal variation is larger at higher latitudes (Halder et al., 2015). This is the opposite of the pattern we observed in Switzerland, where seasonal variation was smaller at higher latitudes. However, in Switzerland, latitude also reflects proximity to the Alps, which has multiple effects on precipitation isotopes and their seasonality. Spatial variations in δ_p seasonality in Switzerland likely reflect differences in cloud processes, moisture sources, and air mass trajectories across this topographically complex landscape (Kern et al., 2014). Beyond affecting air mass trajectories, the topography of the Alps influences the role of convective storms. Convective storms peak in late summer, especially in the Alpine region (Frei et al., 2003), which could explain why there were larger $\delta^{18}\text{O}$ and $\delta^2\text{H}$ amplitudes in the Alpine region; convective storms yield precipitation with high $\delta^{18}\text{O}$ and $\delta^2\text{H}$, and it has been posited that the fraction of convective versus stratiform precipitation may be the primary driver of spatiotemporal variations in precipitation $\delta^{18}\text{O}$ and $\delta^2\text{H}$ (Aggarwal et al., 2016). Alpine topography also influences the recycling of moisture (Froehlich et al., 2008), which may also account for differences in the seasonal cycles of LC-excess from site to site. As such, the correlations between site characteristics and the processes that control δ_p will be specific to individual regions. This provides a rationale for using locally calibrated isoscapes based on site characteristics, even if they do not mechanistically represent the processes that drive variations in δ_p .

The sinusoidal isoscape more accurately represented monthly precipitation $\delta^{18}\text{O}$ than the long-term mean isoscape. The existence of a seasonal cycle implies that the long-term mean isoscape will be a seasonally biased predictor of monthly δ_p (Figure 3a). Furthermore, the spatial variability in the amplitude of δ_p cycles (Figure 2) implies that the spatial gradients in δ_p across the landscape will also vary seasonally. Under

these conditions, long-term mean isoscapes will not accurately reflect spatial gradients in δ_p for specific times of the year. In our study, these spatial gradients were better predicted by sinusoidal or mean monthly isoscapes.

Both the sinusoidal and mean monthly isoscapes yielded similar prediction errors (Figure 3), demonstrating that sine curves can reasonably represent seasonal precipitation $\delta^{18}\text{O}$ variations in Switzerland. An important benefit of the sinusoidal isoscape is that it can be calibrated with sparse or irregular observations of δ_p (Dutton et al., 2005; Jasechko et al., 2016; Wilkinson & Ivany, 2002), which are more readily available than dense, gap-free time series. In contrast to the sinusoidal isoscape, individual-month isoscapes require simultaneous measurements from multiple locations at every time step. However, because the sinusoidal and mean monthly isoscapes are not separately calibrated to every time step, they cannot describe deviations from seasonal patterns, patterns that arise in atypical months or years (Figure 3), or long-term trends (e.g., Stumpp et al., 2014).

Methods that are fitted to individual months, either by regression (the individual-month isoscape), by geostatistical interpolation (the sinusoidal + monthly kriging isoscape), or both (the individual-month + monthly kriging isoscape), intrinsically eliminate the directional biases that arise in many months (Figure 3). These can sometimes be large; for example, the sinusoidal isoscape underestimated precipitation $\delta^{18}\text{O}$ in December 2015 by an average of 3.8‰ due to isotopically anomalous precipitation (Figure 3a). Interstorm and intrastorm variations can be significant in time (e.g., Celle-Jeanton et al., 2001; Coplen et al., 2015; Munksgaard et al., 2012) and space (Fischer et al., 2017), so isotopically anomalous months are likely to be common, and assuming that individual months follow seasonal patterns could be inadequate for some applications. The choice of which monthly calibrated isoscape to use was unimportant here: all of those methods had similar prediction errors (Figure 3).

Though the sinusoidal isoscape was not more accurate than the mean monthly isoscapes in predicting monthly δ_p , it may be a more efficient approach to representing seasonal oscillations because it only requires mapping three sine parameters (i.e., amplitude, ϕ , and offset) rather than constructing 12 independent monthly maps. Furthermore, the sinusoidal isoscape provides continuous δ_p functions that can be evaluated at any point in time, avoiding the need to interpolate between look-up tables, as required with independent monthly maps. This considerably simplifies the task of calculating average isotopic inputs over intervals of particular ecological importance (e.g., growing seasons).

Many of our sites exhibited statistically significant seasonal cycles in LC-excess, although the spatial variations in those cycles could not be effectively predicted by multiple regression on site characteristics. While seasonal cycles in precipitation LC-excess have rarely been described in the literature, recent studies have differed in their attribution of precipitation deuterium excess variations to source effects versus within- and below-cloud processes (Pfahl & Sodemann, 2014; Risi et al., 2013). Regardless of their driving mechanisms, seasonal cycles in LC-excess (with phases offset from those of seasonal cycles of $\delta^{18}\text{O}$ and $\delta^2\text{H}$) are important for many hydrological, climatological, and biological tracer or proxy applications. Although we were unable to effectively predict spatial patterns in the seasonal cycles of LC-excess in Switzerland, ignoring these seasonal cycles could bias the interpretation of LC-excess signals in ecological and hydrological studies. For example, a lake water sample with LC-excess lower than that of mean annual precipitation may be interpreted as implying evaporation, although it may instead simply have come from precipitation that fell during a season with low LC-excess. This example illustrates how quantifying the spatiotemporal variability in precipitation LC-excess may be important for accurately interpreting LC-excess signals in landscapes and ecosystems.

Modeling δ_p as continuous sine curves may be broadly useful for ecological and hydrological applications. In hydrology, the damping and phase shift of seasonal cycles of water isotopes as they propagate through soil profiles or catchments can provide insight into the relative importance of advective and dispersive transport, and thus help constrain models of storage and mixing. Thus, sinusoidal isoscapes are a cornerstone of a new technique for assessing watershed transit-time behavior (the young water fraction; Kirchner, 2016a, 2016b; Jasechko et al., 2016). However, they should also find application in ecology, for example, in determining the origins or quantifying the turnover of water isotope signals in plants and animals (Treydte et al., 2014; Vander Zanden et al., 2014).

5. Conclusions

We demonstrated that seasonal cycles in $\delta^{18}\text{O}$ and $\delta^2\text{H}$ of precipitation (Figure 1) can be represented by sinusoidal cycles and that the parameters describing these sine functions correlate with site characteristics. Multiple regression models based on these characteristics can predict the spatial variations in the seasonality of $\delta^{18}\text{O}$ and $\delta^2\text{H}$ values, which can be mapped as sinusoidal isoscapes (Figures 2 and 3). The sinusoidal isoscape method provided an efficient tool for predicting seasonal and spatial variations in precipitation isotopes across Switzerland. Prediction errors of the sinusoidal isoscape were smaller than those of the long-term mean isoscape but larger than those of isoscapes calibrated individually to each month (Figure 3). We also showed that precipitation LC-excess can exhibit seasonal cycles (Figure 1c). Interpreting $\delta^{18}\text{O}$, $\delta^2\text{H}$, and LC-excess values in soils and biota will often require accounting for seasonal and spatial patterns in water isotopes in precipitation. Sinusoidal isoscapes efficiently encapsulate these patterns, thus providing a promising new tool for isotope studies in hydrology and ecology.

Acknowledgments

We thank Jason West and Rolf Siegwolf for helpful discussions and comments. The data used in this study are publicly available at the URLs listed below. We acknowledge data contributions by the International Atomic Energy Association and GNIP contributors (<http://www.iaea.org/water>), as well as Swiss, German, and Austrian federal monitoring agencies: MeteoSwiss (<http://www.meteo.wiss.admin.ch/>), the Swiss Federal Office for the Environment (FOEN) and its National Groundwater Monitoring Program (NAQUA, its data available on the GNIP database), the Austrian Network of Isotopes in Precipitation (<https://wasser.umweltbundesamt.at/h2odb/>), the Austrian Zentralanstalt für Meteorologie und Geodynamik (<https://www.zamg.ac.at/cms/en/news>), and the Deutscher Wetterdienst (<https://www.dwd.de/>). This project was funded by the Swiss Federal Office for the Environment. G. Goldsmith was supported by funding from the European Community's Seventh Framework Program (FP7-People Marie-Curie Actions/2007-2013) under grant agreement 290605 (COFUND: PSIFELLOW), while previously working at the Paul Scherrer Institute.

References

- Aggarwal, P. K., Romatschke, U., Araguas-Araguas, L., Belachew, D., Longstaffe, F. J., Berg, P., et al. (2016). Proportions of convective and stratiform precipitation revealed in water isotope ratios. *Nature Geoscience*, *9*(8), 624–629. <https://doi.org/10.1038/ngeo2739>
- Bowen, G. J. (2008). Spatial analysis of the intra-annual variation of precipitation isotope ratios and its climatological corollaries. *Journal of Geophysical Research*, *113*, D05113. <https://doi.org/10.1029/2007JD009295>
- Bowen, G. J., West, J. B., Vaughn, B. H., Dawson, T. E., Ehleringer, J. R., Fogel, M. L., et al. (2009). Isoscapes to address large-scale Earth science challenges. *Eos, Transactions American Geophysical Union*, *90*(13), 109–110. <https://doi.org/10.1029/2009EO130001>
- Cable, J., Ogle, K., & Williams, D. (2011). Contribution of glacier meltwater to streamflow in the Wind River Range, Wyoming, inferred via a Bayesian mixing model applied to isotopic measurements. *Hydrological Processes*, *25*(14), 2228–2236. <https://doi.org/10.1002/hyp.7982>
- Celle-jeanton, H., Travi, Y., & Blavoux, B. (2001). Isotopic typology of the precipitation in the western Mediterranean region at three different time scales. *Geophysical Research Letters*, *28*(7), 1215–1218. <https://doi.org/10.1029/2000GL012407>
- Coplen, T. B., Neiman, P. J., White, A. B., & Ralph, F. M. (2015). Categorisation of northern California rainfall for periods with and without a radar brightband using stable isotopes and a novel automated precipitation collector. *Tellus B*, *67*(1). <https://doi.org/10.3402/tellusb.v67.28574>
- Dansgaard, W. (1964). Stable isotopes in precipitation. *Tellus*, *16*(4), 436–468. <https://doi.org/10.1111/j.2153-3490.1964.tb00181.x>
- Delavau, C., Chun, K. P., Stadnyk, T., Birks, S. J., & Welker, J. M. (2015). North American precipitation isotope ($\delta^{18}\text{O}$) zones revealed in time series modeling across Canada and northern United States. *Water Resources Research*, *51*, 1284–1299. <https://doi.org/10.1002/2014WR015687>
- Dutton, A., Wilkinson, B. H., Welker, J. M., Bowen, G. J., & Lohmann, K. C. (2005). Spatial distribution and seasonal variation in $^{18}\text{O}/^{16}\text{O}$ of modern precipitation and river water across the conterminous USA. *Hydrological Processes*, *19*(20), 4121–4146. <https://doi.org/10.1002/hyp.5876>
- Fischer, B. M. C., van Meerveld, H. J., & Seibert, J. (2017). Spatial variability in the isotopic composition of rainfall in a small headwater catchment and its effect on hydrograph separation. *Journal of Hydrology*, *547*, 755–769. <https://doi.org/10.1016/j.jhydrol.2017.01.045>
- Frei, C., Christensen, J. H., Déqué, M., Jacob, D., Jones, R. G., & Vidale, P. L. (2003). Daily precipitation statistics in regional climate models: Evaluation and intercomparison for the European Alps. *Journal of Geophysical Research*, *108*(D3), 4124. <https://doi.org/10.1029/2002JD002287>
- Froehlich, K., Kralik, M., Papesch, W., Rank, D., Scheifinger, H., & Stichler, W. (2008). Deuterium excess in precipitation of Alpine regions—Moisture recycling. *Isotopes in Environmental and Health Studies*, *44*(1), 61–70. <https://doi.org/10.1080/10256010801887208>
- Halder, J., Terzer, S., Wassenaar, L. I., Araguás-Araguás, L. J., & Aggarwal, P. K. (2015). The Global Network of Isotopes in Rivers (GNIR): Integration of water isotopes in watershed observation and riverine research. *Hydrology and Earth System Sciences*, *19*(8), 3419–3431. <https://doi.org/10.5194/hess-19-3419-2015>
- Hobson, K. A., & Wassenaar, L. I. (Eds.) (2008). *Tracking animal migration with stable isotopes*. Amsterdam: Academic Press.
- International Atomic Energy Agency/World Meteorological Organization (2018). Global network of isotopes in precipitation. The GNIP Database. Retrieved from <http://www.iaea.org/water>
- Ingraham, N. L. (1998). Isotopic variations in precipitation. In C. Kendall & J. J. McDonnell (Eds.), *Isotope Tracers in Catchment Hydrology* (pp. 87–118). Amsterdam: Elsevier Science. <https://doi.org/10.1016/B978-0-444-81546-0.50010-0>
- Jasechko, S., Kirchner, J. W., Welker, J. M., & McDonnell, J. J. (2016). Substantial proportion of global streamflow less than three months old. *Nature Geoscience*, *9*(2), 126–129. <https://doi.org/10.1038/ngeo2636>
- Jasechko, S., Sharp, Z. D., Gibson, J. J., Birks, S. J., Yi, Y., & Fawcett, P. J. (2013). Terrestrial water fluxes dominated by transpiration. *Nature*, *496*(7445), 347–350. <https://doi.org/10.1038/nature11983>
- Kern, Z., Kohán, B., & Leuenberger, M. (2014). Precipitation isoscape of high reliefs: Interpolation scheme designed and tested for monthly resolved precipitation oxygen isotope records of an Alpine domain. *Atmospheric Chemistry and Physics*, *14*(4), 1897–1907. <https://doi.org/10.5194/acp-14-1897-2014>
- Kirchner, J. W. (2016a). Aggregation in environmental systems—Part 1: Seasonal tracer cycles quantify young water fractions, but not mean transit times, in spatially heterogeneous catchments. *Hydrology and Earth System Sciences*, *20*(1), 279–297. <https://doi.org/10.5194/hess-20-279-2016>
- Kirchner, J. W. (2016b). Aggregation in environmental systems—Part 2: Catchment mean transit times and young water fractions under hydrologic nonstationarity. *Hydrology and Earth System Sciences*, *20*(1), 299–328. <https://doi.org/10.5194/hess-20-299-2016>
- Landwehr, J. M., & Coplen, T. B. (2006). Line-conditioned excess: A new method for characterizing stable hydrogen and oxygen isotope ratios in hydrologic systems. In *Isotopes in Environmental Studies, Proceedings of an International Conference Held in Monaco 25–29 October 2004* (pp. 132–135). Vienna, Austria: International Atomic Energy Agency.
- Liu, Z., Bowen, G. J., & Welker, J. M. (2010). Atmospheric circulation is reflected in precipitation isotope gradients over the conterminous United States. *Journal of Geophysical Research*, *115*, D22120. <https://doi.org/10.1029/2010JD014175>

- Martin, N. J., Conroy, J. L., Noone, D., Cobb, K. M., Konecky, B. L., & Rea, S. (2018). Seasonal and ENSO influences on the stable isotopic composition of Galápagos precipitation. *Journal of Geophysical Research: Atmospheres*, *123*, 261–275. <https://doi.org/10.1002/2017JD027380>
- McCarroll, D., & Loader, N. J. (2004). Stable isotopes in tree rings. *Quaternary Science Reviews*, *23*(7–8), 771–801. <https://doi.org/10.1016/j.quascirev.2003.06.017>
- Munksgaard, N. C., Wurster, C. M., Bass, A., & Bird, M. I. (2012). Extreme short-term stable isotope variability revealed by continuous rainwater analysis. *Hydrological Processes*, *26*(23), 3630–3634. <https://doi.org/10.1002/hyp.9505>
- Pfahl, S., & Sodemann, H. (2014). What controls deuterium excess in global precipitation? *Climate of the Past*, *10*(2), 771–781. <https://doi.org/10.5194/cp-10-771-2014>
- Risi, C., Noone, D., Frankenberg, C., & Worden, J. (2013). Role of continental recycling in intraseasonal variations of continental moisture as deduced from model simulations and water vapor isotopic measurements. *Water Resources Research*, *49*, 4136–4156. <https://doi.org/10.1002/wrcr.20312>
- Rozanski, K., Araguás-Araguás, L., & Gonfiantini, R. (1993). Isotopic patterns in modern global precipitation. In P. K. Swart, K. C. Lohmann, J. Mckenzie, & S. Savin (Eds.), *Climate Change in Continental Isotopic Records* (Chap. 1, pp. 1–36). Washington, DC: American Geophysical Union. <https://doi.org/10.1029/GM078p0001>
- Sánchez-Murillo, R., & Birkel, C. (2016). Groundwater recharge mechanisms inferred from isoscapes in a complex tropical mountainous region. *Geophysical Research Letters*, *43*, 5060–5069. <https://doi.org/10.1002/2016GL068888>
- Stumpp, C., Klaus, J., & Stichler, W. (2014). Analysis of long-term stable isotopic composition in German precipitation. *Journal of Hydrology*, *517*, 351–361. <https://doi.org/10.1016/j.jhydrol.2014.05.034>
- Treydte, K., Boda, S., Graf Pannatier, E., Fonti, P., Frank, D., Ullrich, B., et al. (2014). Seasonal transfer of oxygen isotopes from precipitation and soil to the tree ring: Source water versus needle water enrichment. *New Phytologist*, *202*(3), 772–783. <https://doi.org/10.1111/nph.12741>
- Vachon, R. W., White, J. W. C., Gutmann, E., & Welker, J. M. (2007). Amount-weighted annual isotopic ($\delta^{18}\text{O}$) values are affected by the seasonality of precipitation: A sensitivity study. *Geophysical Research Letters*, *34*, L21707. <https://doi.org/10.1029/2007GL030547>
- Vander Zanden, H. B., Wunder, M. B., Hobson, K. A., Van Wilgenburg, S. L., Wassenaar, L. I., Welker, J. M., & Bowen, G. J. (2014). Contrasting assignment of migratory organisms to geographic origins using long-term versus year-specific precipitation isotope maps. *Methods in Ecology and Evolution*, *5*(9), 891–900. <https://doi.org/10.1111/2041-210X.12229>
- Wilkinson, B. H., & Ivany, L. C. (2002). Paleoclimatic inference from stable isotope profiles of accretionary biogenic hardparts—A quantitative approach to the evaluation of incomplete data. *Palaeogeography, Palaeoclimatology, Palaeoecology*, *185*(1–2), 95–114. [https://doi.org/10.1016/S0031-0182\(02\)00279-1](https://doi.org/10.1016/S0031-0182(02)00279-1)
- Water Information System Austria (2018). Austrian network of isotopes in precipitation. The Water Information System Austria (WISA) database. Retrieved from <https://wasser.umweltbundesamt.at/h2oddb/>